Review of Particle Physics

REVIEW OF PARTICLE PHYSICS*

Particle Data Group

Abstract

The *Review* summarizes much of particle physics and cosmology. Using data from previous editions, plus 3,062 new measurements from 721 papers, we list, evaluate, and average measured properties of gauge bosons and the recently discovered Higgs boson, leptons, quarks, mesons, and baryons. We summarize searches for hypothetical particles such as supersymmetric particles, heavy bosons, axions, dark photons, etc. All the particle properties and search limits are listed in Summary Tables. We also give numerous tables, figures, formulae, and reviews of topics such as Higgs Boson Physics, Supersymmetry, Grand Unified Theories, Neutrino Mixing, Dark Energy, Dark Matter, Cosmology, Particle Detectors, Colliders, Probability and Statistics. Among the 117 reviews are many that are new or heavily revised, including new reviews on Pentaquarks and Inflation.

The complete *Review* is published online in a journal and on the website of the Particle Data Group (`http://pdg.lbl.gov`). The printed *PDG Book* contains the Summary Tables and all review articles but no longer includes the detailed tables from the Particle Listings. A *Booklet* with the Summary Tables and abbreviated versions of some of the review articles is also available.

DOI: 10.1088/1674-1137/40/10/100001

The 2016 edition of *Review of Particle Physics* should be cited as:
C. Patrignani et al. (Particle Data Group), Chinese Physics C, **40**, 100001 (2016)

*The publication of the *Review of Particle Physics* is supported by the Director, Office of Science, Office of High Energy Physics of the U.S. Department of Energy under Contract No. DE–AC02–05CH11231; by the European Laboratory for Particle Physics (CERN); by an implementing arrangement between the governments of Japan (MEXT: Ministry of Education, Culture, Sports, Science and Technology) and the United States (DOE) on cooperative research and development; by the Institute of High Energy Physics, Chinese Academy of Sciences; and by the Italian National Institute of Nuclear Physics (INFN).

Particle Data Group

C. Patrignani,[1] K. Agashe,[2] G. Aielli,[3] C. Amsler,[4,5] M. Antonelli,[6] D.M. Asner,[7] H. Baer,[8] Sw. Banerjee,[9] R.M. Barnett,[10] T. Basaglia,[11] C.W. Bauer,[10] J.J. Beatty,[12] V.I. Belousov,[13] J. Beringer,[10] S. Bethke,[14] H. Bichsel,[15] O. Biebel,[16] E. Blucher,[17] G. Brooijmans,[18] O. Buchmueller,[19] V. Burkert,[20] M.A. Bychkov,[21] R.N. Cahn,[10] M. Carena,[22,17,23] A. Ceccucci,[11] A. Cerri,[24] D. Chakraborty,[25] M.-C. Chen,[26] R.S. Chivukula,[27] K. Copic,[10] G. Cowan,[28] O. Dahl,[10] G. D'Ambrosio,[29] T. Damour,[30] D. de Florian,[31] A. de Gouvêa,[32] T. DeGrand,[33] P. de Jong,[34] G. Dissertori,[35] B.A. Dobrescu,[22] M. D'Onofrio,[36] M. Doser,[11] M. Drees,[37] H.K. Dreiner,[37] D.A. Dwyer,[10] P. Eerola,[38,39] S. Eidelman,[40,41] J. Ellis,[42,11] J. Erler,[43] V.V. Ezhela,[13,44] W. Fetscher,[35] B.D. Fields,[45,46] B. Foster,[47,48,49] A. Freitas,[50] H. Gallagher,[51] L. Garren,[22] H.-J. Gerber,[35] G. Gerbier,[52] T. Gershon,[53] T. Gherghetta,[54] A.A. Godizov,[13] M. Goodman,[55] C. Grab,[35] A.V. Gritsan,[56] C. Grojean,[57] D.E. Groom,[10] M. Grünewald,[58] A. Gurtu,[59,11] T. Gutsche,[60] H.E. Haber,[61] K. Hagiwara,[62] C. Hanhart,[63] S. Hashimoto,[62] Y. Hayato,[64] K.G. Hayes,[65] A. Hebecker,[66] B. Heltsley,[67] J.J. Hernández-Rey,[68] K. Hikasa,[69] J. Hisano,[70] A. Höcker,[11] J. Holder,[71,72] A. Holtkamp,[11] J. Huston,[27] T. Hyodo,[73] K. Irwin,[74,75] J.D. Jackson,[10†] K.F. Johnson,[76] M. Kado,[77,11] M. Karliner,[78] U.F. Katz,[79] S.R. Klein,[80] E. Klempt,[81] R.V. Kowalewski,[82] F. Krauss,[83] M. Kreps,[53] B. Krusche,[84] Yu.V. Kuyanov,[13] Y. Kwon,[85] O. Lahav,[86] J. Laiho,[87] P. Langacker,[88] A. Liddle,[89] Z. Ligeti,[10] C.-J. Lin,[10] C. Lippmann,[90] T.M. Liss,[91] L. Littenberg,[92] K.S. Lugovsky,[10,13] S.B. Lugovsky,[13] A. Lusiani,[93] Y. Makida,[62] F. Maltoni,[94] T. Mannel,[95] A.V. Manohar,[96] W.J. Marciano,[92] A.D. Martin,[83] A. Masoni,[97] J. Matthews,[98] U.-G. Meißner,[81,63] D. Milstead,[99] R.E. Mitchell,[100] P. Molaro,[101] K. Mönig,[102] F. Moortgat,[11] M.J. Mortonson,[103,10] H. Murayama,[104,105,10] K. Nakamura,[104,62] M. Narain,[106] P. Nason,[107] S. Navas,[108] M. Neubert,[109] P. Nevski,[92] Y. Nir,[110] K.A. Olive,[54] S. Pagan Griso,[10] J. Parsons,[18] J.A. Peacock,[89] M. Pennington,[20] S.T. Petcov,[111,104,112] V.A. Petrov,[13] A. Piepke,[113] A. Pomarol,[114] A. Quadt,[115] S. Raby,[12] J. Rademacker,[116] G. Raffelt,[117] B.N. Ratcliff,[75] P. Richardson,[83] A. Ringwald,[48] S. Roesler,[11] S. Rolli,[118] A. Romaniouk,[119] L.J. Rosenberg,[15] J.L. Rosner,[17] G. Rybka,[15] R.A. Ryutin,[13] C.T. Sachrajda,[120] Y. Sakai,[62] G.P. Salam,[11,121] S. Sarkar,[122,123] F. Sauli,[11] O. Schneider,[124] K. Scholberg,[125] A.J. Schwartz,[126] D. Scott,[127] V. Sharma,[96] S.R. Sharpe,[15] T. Shutt,[75] M. Silari,[11] T. Sjöstrand,[128] P. Skands,[129] T. Skwarnicki,[87] J.G. Smith,[33] G.F. Smoot,[130,105,10] S. Spanier,[131] H. Spieler,[10] C. Spiering,[102] A. Stahl,[132] S.L. Stone,[87] Y. Sumino,[69] T. Sumiyoshi,[133] M.J. Syphers,[25,22] F. Takahashi,[69] M. Tanabashi,[70] K. Terashi,[64] J. Terning,[134] R.S. Thorne,[86] L. Tiator,[135] M. Titov,[52] N.P. Tkachenko,[13] N.A. Törnqvist,[39] D. Tovey,[136] G. Valencia,[129] R. Van de Water,[22] N. Varelas,[17] G. Venanzoni,[6] M.G. Vincter,[137] P. Vogel,[138] A. Vogt,[139] S.P. Wakely,[17,23] W. Walkowiak,[95] C.W. Walter,[125] D. Wands,[140] D.R. Ward,[141] M.O. Wascko,[19] G. Weiglein,[48] D.H. Weinberg,[142] E.J. Weinberg,[18] M. White,[105,10] L.R. Wiencke,[143] S. Willocq,[144] C.G. Wohl,[10] L. Wolfenstein,[145†] J. Womersley,[146] C.L. Woody,[92] R.L. Workman,[147] W.-M. Yao,[10] G.P. Zeller,[22] O.V. Zenin,[13,44] R.-Y. Zhu,[148] F. Zimmermann,[11] P.A. Zyla[10]

Technical Associates: J. Anderson,[10] G. Harper,[10] V.S. Lugovsky,[13] P. Schaffner[10]

1. *Università di Bologna and INFN, Dip. Scienze per la Qualità della Vita, I-47921, Rimini, Italy*
2. *University of Maryland, Department of Physics, College Park, MD 20742-4111, USA*
3. *Universit degli Studi di Roma "Tor Vergata", Via Orazio, Raimondo, 18, 00173 Rome, Italy*
4. *Albert Einstein Center for Fundamental Physics, Universität Bern, CH-3012 Bern, Switzerland*
5. *Stefan Meyer Institute for Subatomic Physics, Austrian Academy of Sciences, Boltzmanngasse 3, 1090 Vienna, Austria*
6. *Lab. Nazionali di Frascati dell'INFN, CP 13, via E. Fermi, 40, I-00044 Frascati (Roma), Italy*
7. *Pacific Northwest National Laboratory, 902 Battelle Boulevard, Richland, WA 99352, USA*
8. *Department of Physics and Astronomy, University of Oklahoma, Norman, OK 73019, USA*
9. *University of Louisville, Louisville, KY 40292, USA*
10. *Physics Division, Lawrence Berkeley National Laboratory, 1 Cyclotron Road, Berkeley, CA 94720, USA*
11. *CERN, European Organization for Nuclear Research, CH-1211 Genève 23, Switzerland*
12. *Department of Physics, The Ohio State University, 191 W. Woodruff Ave., Columbus, OH 43210, USA*
13. *COMPAS Group, Institute for High Energy Physics, RU-142284, Protvino, Russia*
14. *Max-Planck-Institute of Physics, 80805 Munich, Germany*
15. *Department of Physics, University of Washington, Seattle, WA 98195, USA*
16. *Ludwig-Maximilians-Universität, Fakultät für Physik, Schellingstr. 4, D-80799 München, Germany*
17. *Enrico Fermi Institute and Department of Physics, University of Chicago, Chicago, IL 60637-1433, USA*
18. *Department of Physics, Columbia University, 538 W. 120th Street, New York, NY, 10027 USA*
19. *High Energy Physics Group, Blackett Laboratory, Imperial College, Prince Consort Road, London SW7 2AZ, UK*
20. *Jefferson Lab, 12000 Jefferson Ave., Newport News, VA 23606, USA*
21. *Department of Physics, University of Virginia, PO Box 400714, Charlottesville, VA 22904, USA*
22. *Fermi National Accelerator Laboratory, P.O. Box 500, Batavia, IL 60510, USA*
23. *Kavli Institute for Cosmological Physics, University of Chicago, Chicago, IL 60637-1433, USA*
24. *Department of Physics and Astronomy, University of Sussex, Falmer, Brighton BN1 9QH, UK*
25. *Department of Physics, Northern Illinois University, DeKalb, IL 60115, USA*

† Deceased

26. *Department of Physics and Astronomy, University of California, Irvine, CA 92697-4575, USA*
27. *Michigan State University, Dept. of Physics and Astronomy, East Lansing, MI 48824-2320, USA*
28. *Department of Physics, Royal Holloway, University of London, Egham, Surrey TW20 0EX, UK*
29. *INFN - Sezione di Napoli, Complesso Universitario Monte Sant'Angelo, Via Cintia, 80126 Napoli, Italy*
30. *Institut des Hautes Etudes Scientifiques, F-91440 Bures-sur-Yvette, France*
31. *International Center for Advanced Studies (ICAS), UNSAM, 25 de Mayo y Francia, (1650) Buenos Aires, Argentina*
32. *Department of Physics and Astronomy, Northwestern University, Evanston, IL 60208, USA*
33. *Department of Physics, University of Colorado at Boulder, Boulder, CO 80309, USA*
34. *Nikhef, P.O. Box 41882, 1009 DB Amsterdam, and University of Amsterdam, the Netherlands*
35. *Institute for Particle Physics, ETH Zurich, 8093 Zurich, Switzerland*
36. *University of Liverpool, Department of Physics, Oliver Lodge Lab, Oxford St., Liverpool L69 3BX, UK*
37. *Physikalisches Institut, Universität Bonn, Nussallee 12, D-53115 Bonn, Germany*
38. *Helsinki Institute of Physics, POB 64 FI-00014 University of Helsinki, Finland*
39. *Department of Physics, POB 64 FI-00014 University of Helsinki, Finland*
40. *Budker Institute of Nuclear Physics SB RAS, Novosibirsk 630090, Russia*
41. *Novosibirsk State University, Novosibirsk 630090, Russia*
42. *King's College London, Department of Physics, Strand, London, WC2R 2LS, UK*
43. *Departamento de Física Teórica, Instituto de Física, Universidad Nacional Autónoma de México, México D.F. 04510, México*
44. *Moscow Institute of Physics and Technology (State University), RU-141700, Dolgoprudny, Moscow region, Russian Federation*
45. *Department of Astronomy, University of Illinois, 1002 W. Green St., Urbana, IL 61801, USA*
46. *Department of Physics, University of Illinois, 1110 W. Green St., Urbana, IL 61801, USA*
47. *University of Hamburg, Notkestrasse 85, D-22607 Hamburg, Germany*
48. *Deutsches Elektronen-Synchrotron DESY, Notkestraße 85, D-22607 Hamburg, Germany*
49. *Denys Wilkinson Building, Department of Physics, University of Oxford, Oxford, OX1 3RH, UK*
50. *University of Pittsburgh, Department of Physics and Astronomy, 3941 O'Hara St, Pittsburgh, PA 15260, USA*
51. *Department of Physics and Astronomy, Tufts University, 4 Colby Street, Medford, MA 02155, USA*
52. *CEA Saclay, DSM/IRFU/SPP, F-91191 Gif-sur-Yvette, France*
53. *Department of Physics, University of Warwick, Coventry, CV4 7AL, UK*
54. *University of Minnesota, School of Physics and Astronomy, 116 Church St. S.E., Minneapolis, MN 55455, USA*
55. *Argonne National Laboratory, 9700 S. Cass Ave., Argonne, IL 60439-4815, USA*
56. *Johns Hopkins University, Baltimore, Maryland 21218, USA*
57. *Institució Catalana de Recerca i Estudis Avancats, Institut de Física d'Altes Energies, E-08193 Bellaterra (Barcelona), Spain*
58. *School of Physics, University College Dublin, Belfield, Dublin 4, Ireland*
59. *(now retired) TIFR, Homi Bhabha Road, Mumbai, India*
60. *Institut für Theoretische Physik, Universität Tübingen, Auf der Morgenstelle 14, D-72076 Tübingen, Germany*
61. *Santa Cruz Institute for Particle Physics, University of California, Santa Cruz, CA 95064, USA*
62. *KEK, High Energy Accelerator Research Organization, Oho, Tsukuba-shi, Ibaraki-ken 305-0801, Japan*
63. *Institut für Kernphysik and Institute for Advanced Simulation, Forschungszentrum Jülich, Jülich, Germany*
64. *Department of Physics, University of Tokyo, Tokyo 113-0033, Japan*
65. *Department of Physics, Hillsdale College, Hillsdale, MI 49242, USA*
66. *Institute for Theoretical Physics, Heidelberg University, Philosophenweg 19, D-69120 Heidelberg, Germany*
67. *Laboratory of Elementary-Particle Physics, Cornell University, Ithaca, NY 14853, USA*
68. *IFIC — Instituto de Física Corpuscular, Universitat de València — C.S.I.C., E-46071 València, Spain*
69. *Department of Physics, Tohoku University, Aoba-ku, Sendai 980-8578, Japan*
70. *Kobayashi-Maskawa Institute, Nagoya University, Chikusa-ku, Nagoya 464-0028, Japan*
71. *Department of Physics and Astronomy, University of Delaware, Newark, DE 19716, USA*
72. *Bartol Research Institute, University of Delaware, Newark, DE 19716, USA*
73. *Yukawa Institute for Theoretical Physics, Kyoto University, Kitashirakawa Oiwakecho, Sakyo-ku, Kyoto, 606-8502, Japan*
74. *Department of Physics, Stanford University, Stanford, CA 94305, USA*
75. *SLAC National Accelerator Laboratory, 2575 Sand Hill Road, Menlo Park, CA 94025, USA*
76. *Los Alamos National Laboratory, Los Alamos, NM 87545, USA*
77. *LAL, IN2P3-CNRS et Univ. de Paris 11, F-91898 Orsay CEDEX, France*
78. *Department of Particle Physics, Tel-Aviv University, Ramat Aviv, Tel Aviv 69978, Israel*
79. *University of Erlangen-Nuremberg, Erlangen Centre for Astroparticle Physics, Erwin-Rommel-Str. 1, 91058 Erlangen, Germany*

80. *Nuclear Science Division, Lawrence Berkeley National Laboratory, 1 Cyclotron Road, Berkeley, CA 94720, USA*
81. *Helmholtz-Institut für Strahlen- und Kernphysik, Universität Bonn, Nussallee 14–16, D-53115 Bonn, Germany*
82. *University of Victoria, Victoria, BC V8W 3P6, Canada*
83. *Institute for Particle Physics Phenomenology, Department of Physics, University of Durham, Durham DH1 3LE, UK*
84. *Institute of Physics, University of Basel, CH-4056 Basel, Switzerland*
85. *Yonsei University, Department of Physics, 134 Sinchon-dong, Sudaemoon-gu, Seoul 120-749, South Korea*
86. *Department of Physics and Astronomy, University College London, Gower Street, London WC1E 6BT, UK*
87. *Department of Physics, Syracuse University, Syracuse, NY, 13244, USA*
88. *School of Natural Science, Institute for Advanced Study, Princeton, NJ 08540, USA*
89. *Institute for Astronomy, University of Edinburgh, Royal Observatory, Blackford Hill, Edinburgh, EH9 3HJ, Scotland, UK*
90. *GSI, Helmholtzzentrum für Schwerionenforschung, Darmstadt, Germany*
91. *Division of Science, City College of New York, 160 Convent Avenue, New York, NY 10031*
92. *Physics Department, Brookhaven National Laboratory, Upton, NY 11973, USA*
93. *INFN and Dipartimento di Fisica, Universitá di Pisa, I-56127 Pisa, Italy*
94. *Centre for Cosmology, Particle Physics and Phenomenology (CP3), Université catholique de Louvain, B-1348 Louvain-la-Neuve, Belgium*
95. *Department für Physik, Universität Siegen, Walter-Flex-Str. 3, 57068 Siegen, Germany*
96. *Department of Physics, University of California at San Diego, La Jolla, CA 92093, USA*
97. *INFN Sezione di Cagliari, Cittadella Universitaria di Monserrato, I-09042 Monserrato (CA), Italy*
98. *Department of Physics and Astronomy, Louisana State University, Baton Rouge, LA 70803, USA*
99. *Fysikum, Stockholms Universitet, AlbaNova University Centre, SE-106 91 Stockholm, Sweden*
100. *Deparment of Physics, Indiana University, 727 E. 3rd St., Bloomington, IN 47405-7105, USA*
101. *INAF-OATS, via G.B. Tiepolo 11, 34143 Trieste, Italy*
102. *DESY, D-15735 Zeuthen, Germany*
103. *The Space Sciences Laboratory (SSL), University of California, 7 Gauss Way, Berkeley, CA 94720, USA*
104. *Kavli IPMU (WPI), Todai Institutes for Advanced Study, University of Tokyo, Kashiwa, Chiba 277-8583, Japan*
105. *Department of Physics, University of California, Berkeley, CA 94720, USA*
106. *Brown University, Department of Physics, 182 Hope Street, Providence, RI 02912, USA*
107. *INFN, Sez. di Milano-Bicocca, Piazza della Scienza, 3, I-20126 Milano, Italy*
108. *Dpto. de Física Teórica y del Cosmos & C.A.F.P.E., Universidad de Granada, 18071 Granada, Spain*
109. *PRISMA Cluster of Excellence and Mainz Institute for Theoretical Physics, Johannes Gutenberg University, D-55099 Mainz, Germany*
110. *Department of Particle Physics and Astrophysics, Weizmann Institute of Science, Rehovot 7610001, Israel*
111. *SISSA/INFN, via Bonomea, 265, 34136 Trieste TS, Italy*
112. *INRNE, Bulgarian Academy of Sciences, 1784 Sofia, Bulgaria*
113. *Department of Physics and Astronomy, University of Alabama, 206 Gallalee Hall, Tuscaloosa, AL 35487, USA*
114. *Departament de Física, Universitat Autonòma de Barcelona, 08193 Bellaterra, Barcelona, Spain*
115. *Georg-August-Universität Göttingen, II. Physikalisches Institut, Friedrich-Hund-Platz 1, D-37077 Göttingen, Germany*
116. *HH Wills Physics Laboratory, University of Bristol, Tyndall Avenue, Bristol BS8 1TL, UK*
117. *Max-Planck-Institut für Physik (Werner-Heisenberg-Institut), Föhringer Ring 6, D-80805 München, Germany*
118. *DOE, 1000 Independence Ave, SW, SC-25 Germantown Bldg, Washington, DC 20585, USA*
119. *National Research Nuclear University "MEPhI" (Moscow Engineering Physics Institute), 31, Kashirskoye shosse, 115409 Moscow, Russia*
120. *School of Physics and Astronomy, University of Southampton, Highfield, Southampton S017 1BJ, UK*
121. *(on leave from) LPTHE, UPMC Université de Paris 6, CNRS UMR 7589, 4 place Jussieu, Paris, France*
122. *Rudolf Peierls Centre for Theoretical Physics, University of Oxford, 1 Keble Road, Oxford OX1 3NP, UK*
123. *Niels Bohr Institute, Blegdamsvej 17, 2100 Copenhagen, Denmark*
124. *Ecole Polytechnique Fédérale de Lausanne (EPFL), CH-1015 Lausanne, Switzerland*
125. *Physics Department, Duke University, Durham, NC 27708, USA*
126. *Department of Physics, University of Cincinnati, 400 Geology/Physics Bldg., Cincinnati, OH 45221-0377, USA*
127. *Department of Physics and Astronomy, University of British Columbia, Vancouver, BC V6T 1Z1, Canada*
128. *Department of Astronomy and Theoretical Physics, Lund University, S-223 62 Lund, Sweden*
129. *School of Physics, Monash University, Melbourne, Victoria 3800, Australia*
130. *Paris Centre for Cosmological Physics, APC (CNRS), Université Paris Diderot, Université Sorbonne Paris Cité, Paris 75013 France*
131. *Department of Physics and Astronomy, University of Tennessee, Knoxville, TN 37996, USA*
132. *III. Physikalisches Institut, Physikzentrum, RWTH Aachen University, 52056 Aachen, Germany*
133. *High Energy Physics Laboratory, Tokyo Metropolitan University, Tokyo, 192-0397, Japan*

134. *Department of Physics, University of California, Davis, CA 95616, USA*
135. *Institut für Kernphysik, Johannes-Gutenberg Universität Mainz, D-55099 Mainz, Germany*
136. *Department of Physics and Astronomy, University of Sheffield, Sheffield S3 7RH, UK*
137. *Department of Physics, Carleton University, 1125 Colonel By Drive, Ottawa, ON K1S 5B6, Canada*
138. *California Institute of Technology, Kellogg Radiation Laboratory 106-38, Pasadena, CA 91125, USA*
139. *Division of Theoretical Physics, Department of Mathematical Sciences, The University of Liverpool, Liverpool, L69 3BX, UK*
140. *Institute of Cosmology and Gravitation, University of Portsmouth, Burnaby Road, Portsmouth PO1 3FX, UK*
141. *Cavendish Laboratory, J.J. Thomson Avenue, Cambridge CB3 0HE, UK*
142. *Department of Astronomy and CCAPP, The Ohio State University, 140 W. 18th Ave., Columbus, OH 43210, USA*
143. *Dept. of Physics, Colorado School of Mines, Golden Colorado, 80401 USA*
144. *Department of Physisc, University of Massachusetts, Amherst, 1126 Lederle Graduate Research Tower, Amherst, MA 01003-4525, USA*
145. *Department of Physics, Carnegie Mellon University, Pittsburgh, PA 15213, USA*
146. *STFC Rutherford Appleton Laboratory, Didcot, OX11 0QX, UK*
147. *Department of Physics, George Washington University Virginia Campus, Ashburn, VA 20147-2604, USA*
148. *California Institute of Technology, High Energy Physics, MC 256-48, Pasadena, CA 91125, USA*

HIGHLIGHTS OF THE 2016 EDITION OF THE REVIEW OF PARTICLE PHYSICS

721 new papers with 3062 new measurements

- Over 332 new papers from **LHC** experiments (ATLAS, CMS, and LHCb).
- Extensive up-to-date **Higgs boson** coverage from 79 new papers with 172 measurements.
- **Supersymmetry**: 82 new papers with major exclusions.
- **Top quark**: 55 new papers.
- Latest from ***B*-meson** physics: 133 papers with 542 measurements.
- New τ **branching fractions** fit in collaboration with the HFAG-Tau group.
- New limits on neutrinoless **double-β decays**.
- Updated and new results in **neutrino mixing** on Δm^2 and mixing angle measurements.
- Experimental Tests of Gravitational Theory review includes LIGO observation of **gravitational waves**.
- Cosmology reviews updated to include **2015 Planck** results.
- **Periodic Table** 7th row completed; significantly revised Atomic-Nuclear Properties website.

117 reviews (most are revised)

- **New reviews** on:
  - Inflation
  - Pentaquarks
  - Pole Structure of the $\Lambda(1405)$ Region
- **Significant update/revision** to reviews on:
  - Higgs Boson Physics
  - Grand Unified Theories
  - Dark Energy, Dark Matter and CMB
  - Cosmological Parameters, Astrophysical Constants and Parameters
  - Neutrino Mass, Mixing, and Flavor Change
  - Neutrino Cross Section Measurements
  - W' and Z' bosons searches
  - Searches for Quark and Lepton Compositeness
  - Leptonic Decays of Charged Pseudoscalar Mesons
  - Particle Detectors for accelerator and non-accelerator physics, including new section on Accelerator Neutrino Detectors
  - High-Energy Collider Parameters

See **pdgLive.lbl.gov** for online access to PDG database.

See **pdg.lbl.gov/AtomicNuclearProperties** for Atomic Properties of Materials.

TABLE OF CONTENTS

(Continued on next page.)

PARTICLE LISTINGS*

MAJOR REVIEWS IN THE PARTICLE LISTINGS

*The divider sheets give more detailed indices for each main section of the Particle Listings.

a characteristic length X_0 and the other with length λ_I [173]. Fits to this 4-parameter function are commonly used, *e.g.*, by the ATLAS Tilecal collaboration [165]. If the interaction point is not known (the usual case), the distribution must be convoluted with an exponential in the interaction length of the incident particle. Adragna *et al.* give an analytic form for the convoluted function [165].

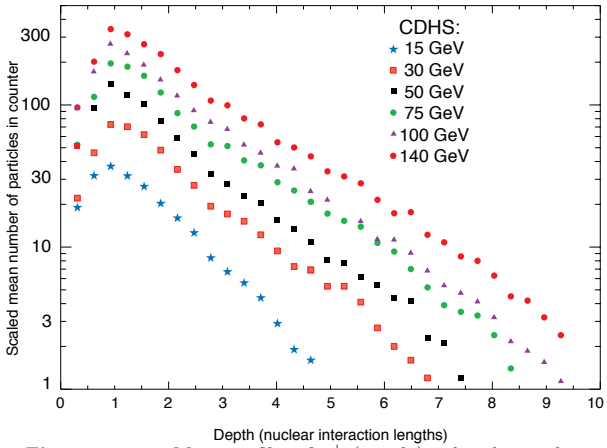

Figure 34.24: Mean profiles of π^+ (mostly) induced cascades in the CDHS neutrino detector [172]. Corresponding results for the ATLAS tile calorimeter can be found in Ref. 165.

The transverse energy deposit is characterized by a central core dominated by EM cascades, together with a wide "skirt" produced by wide-angle hadronic interactions [174].

The CALICE collaboration has tested a "tracking" calorimeter (AHCAL) with highly granular scintillator readout [161]. Since the position of the first interaction is observed, the average longitudinal and radial shower distributions are obtained.

While the average distributions might be useful in designing a calorimeter, they have little meaning for individual events, whose distributions are extremely variable because of the small number of particles involved early in the cascade.

Particle identification, primarily e-π discrimination, is accomplished in most calorimeters by depth development. An EM shower is mostly contained in $15X_0$ while a hadronic shower takes about $4\lambda_I$. In high-A absorbers such as Pb, $X_0/\lambda_I \sim 0.03$. In a fiber calorimeter, such as the RD52 dual-readout calorimeter [175], e-π discrimination is achieved by differences in the Cerenkov and scintillation signals, lateral spread, and timing differences, ultimately achieving about 500:1 discrimination.

34.9.3. *Free electron drift velocities in liquid ionization chambers* :

Written August 2009 by W. Walkowiak (U. Siegen)

Drift velocities of free electrons in LAr [176] are given as a function of electric field strength for different temperatures of the medium in Fig. 34.25. The drift velocites in LAr have been measured using a double-gridded drift chamber with electrons produced by a laser pulse on a gold-plated cathode. The average temperature gradient of the drift velocity of the free electrons in LAr is described [176] by

$$\frac{\Delta v_d}{\Delta T\, v_d} = (-1.72 \pm 0.08)\ \%/\mathrm{K}.$$

Earlier measurements [177–180] used different techniques and show systematic deviations of the drift velocities for free electrons which cannot be explained by the temperature dependence mentioned above.

Drift velocities of free electrons in LXe [178] as a function of electric field strength are also displayed in Fig. 34.25. The drift velocity saturates for $|\boldsymbol{E}| > 3$ kV/cm, and decreases with increasing temperature for LXe as well as measured e.g. by [181].

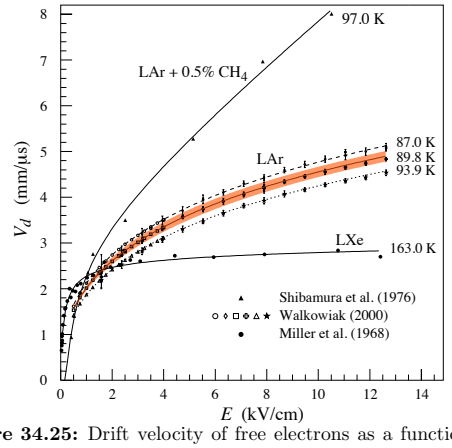

Figure 34.25: Drift velocity of free electrons as a function of electric field strength for LAr [176], LAr + 0.5% CH_4 [178] and LXe [177]. The average temperatures of the liquids are indicated. Results of a fit to an empirical function [182] are superimposed. In case of LAr at 91 K the error band for the global fit [176] including statistical and systematic errors as well as correlations of the data points is given. Only statistical errors are shown for the individual LAr data points.

The addition of small concentrations of other molecules like N_2, H_2 and CH_4 in solution to the liquid typically increases the drift velocities of free electrons above the saturation value [178,179], see example for CH_4 admixture to LAr in Fig. 34.25. Therefore, actual drift velocities are critically dependent on even small additions or contaminations.

34.10. Accelerator Neutrino Detectors

Written August 2015 by M.O. Wascko (Imperial College London).

34.10.1. *Introduction* :

Accelerator neutrino experiments span many orders of magnitude in neutrino energy, from a few MeV to hundreds of GeV. This wide range of neutrino energy is driven by the many physics applications of accelerator neutrino beams. Foremost among them is neutrino oscillation, which varies as the ratio L/E_ν, where L is the neutrino baseline (distance travelled), and E_ν is the neutrino energy. But accelerator neutrino beams have also been used to study the nature of the weak interaction, to probe nucleon form factors and structure functions, and to study nuclear structure.

The first accelerator neutrino experiment used neutrinos from the decays of high energy pions in flight to show that the neutrinos emitted from pion decay are different from the neutrinos emitted by beta decay [183]. The field of accelerator neutrino experiments did not expand beyond this until Simon van der Meer's invention of the magnetic focusing horn [184], which significantly increased the flux of neutrinos aimed toward the detector. In this mini-review, we focus on experiments employing decay-in-flight beams—pions, kaons, charmed mesons, and taus—producing fluxes of neutrinos and antineutrinos from $\sim$ 10 MeV to $\sim$ 100 GeV.

Neutrino interactions with matter proceed only through the weak interaction, making the cross section extremely small and requiring high fluxes of neutrinos and large detector masses in order to achieve satisfactory event rates. Therefore, neutrino detector design is a balancing act taking into account sufficient numbers of nuclear targets (often achieved with inactive detector materials), adequate sampling/segmentation to ensure accurate reconstruction of the tracks and showers produced by neutrino-interaction secondary particles, and practical readout systems to allow timely analysis of data.

34.10.2. ***Signals and Backgrounds*** :

The neutrino interaction processes available increase with increasing neutrino energy as interaction thresholds are crossed; in general neutrino-interaction cross sections grow with energy; for a detailed discussion of neutrino interactions see [185]. The multiplicity of secondary particles from each interaction process grows in complexity with neutrino energy, while the forward-boost due to increasing E_ν compresses the occupied phase space in the lab frame, impacting detector designs. Because decay-in-fight beams produce neutrinos at well-defined times, leading to very small duty factors, the predominant backgrounds stem from unwanted beam-induced neutrino interactions, i.e. neutrinos interacting via other processes than the one being studied. This becomes increasingly true at high energies because the secondary particles produced by neutrino interactions yield detector signals that resemble cosmic backgrounds less and less.

Below, we describe a few of the dominant neutrino interaction processes, with a focus on the final state particle content and topologies.

34.10.2.1. *Charged-Current Quasi-Elastic Scattering and Pions:*

Below $\sim$ 2 GeV neutrino energy, the dominant neutrino-nucleus interaction process is quasi-elastic (QE) scattering. In the charged current (CC) mode, the CCQE base neutrino reaction is $\nu_\ell\, n \to \ell^-\, p$, where $\ell = e, \mu, \tau$, and similarly for antineutrinos, $\overline{\nu}_\ell\, p \to \ell^+\, n$. The final state particles are a charged lepton, and perhaps a recoiling nucleon if it is given enough energy to escape the nucleus. Detectors designed to observe this process should have good single-particle track resolution for muon neutrino interactions, but should have good μ/e separation for electron neutrino interactions. Because the interaction cross section falls sharply with Q^2, the lepton typically carries away more of the neutrino's kinetic energy than the recoiling nucleon. The fraction of backward-scattered leptons is large, however, so detectors with 4π coverage are desirable. The dominant backgrounds in this channel tend to come from single pion production events in which the pion is not detected.

Near 1 GeV, the quasi-elastic cross section is eclipsed by pion production processes. A typical single pion production (CC1π) reaction is $\nu_\ell\, n \to \ell^-\, \pi^+\, n$, but many more final state particle combinations are possible. Single pion production proceeds through the coherent channel and many incoherent processes, dominated by resonance production. With increasing neutrino energy, higher-order resonances can be excited, leading to multiple pions in the final state. Separating these processes from quasi-elastic scattering, and indeed from each other, requires tagging, and ideally reconstructing, the pions. Since these processes can produce neutral pions, electromagnetic (EM) shower reconstruction is more important here than it is for the quasi-elastic channel. The predominant backgrounds for pion production change with increasing neutrino energy. Detection of pion processes is also complicated because near threshold the quasi-elastic channel creates pion backgrounds through final state interactions of the recoiling nucleon, and at higher energies backgrounds come from migration of multiple pion events in which one or more pions is not detected.

34.10.2.2. *Deep Inelastic Scattering:*

Beyond a few GeV, the neutrino has enough energy to probe the nucleon at the parton scale, leading to deep inelastic scattering (DIS). In the charged-current channel, the DIS neutrino reaction is $\nu_\ell\, N \to \ell^-\, X$, where N is a nucleon and X encompasses the entire recoiling hadronic system. The final state particle reconstruction revolves around accurate reconstruction of the lepton momentum and containment and reconstruction of the hadronic shower energy. Because of the high neutrino energies involved, DIS events are very forward boosted, and can have extremely long particle tracks. For this reason, detectors measuring DIS interactions must be large to contain the hadronic showers in the detector volume.

34.10.2.3. *Neutral Currents:*

Neutrino interactions proceeding through the neutral current (NC) channel are identified by the lack of a charged lepton in the final state. For example, the NC elastic reaction is $\nu_l\, N \to \nu_l\, N$, and the NC DIS reaction is $\nu_l\, N \to \nu_l\, X$. NC interactions are suppressed relative to CC interactions by a factor involving the weak mixing angle; the primary backgrounds for NC interactions come from CC interactions in which the charged lepton is misidentified.

34.10.3. ***Instances of Neutrino Detector Technology*** :

Below we describe many of the actual detectors that have been built and operated for use in accelerator neutrino beams.

34.10.3.1. *Spark Chambers:*

In the first accelerator neutrino beam experiment, Lederman, Schwartz, and Steinberger [183] used an internally-triggered spark chamber detector, filled with 10 tons of Al planes and surrounded by external scintillator veto planes, to distinguish muon tracks from electron showers, and hence muon neutrinos from electron neutrinos. The inactive Al planes served as the neutrino interaction target and as radiators for EM shower development. The detector successfully showed the presence of muon tracks from neutrino interactions. It was also sensitive to the hadronic showers induced by NC interactions, which were unknown at the time. More than a decade later, the Aachen-Padova [186] experiment at CERN also employed an Al spark chamber to detect $\sim$ 2 GeV neutrinos.

34.10.3.2. *Bubble Chambers:*

Several large bubble chamber detectors were employed as accelerator neutrino detectors in the 1970s and 80s, performing many of the first studies of the properties of the weak interaction. Bubble chambers provide exquisite granularity in the reconstruction of secondary particles, allowing very accurate separation of interaction processes. However, the extremely slow and labor-intensive acquisition and analysis of the data from photographic film led to them being phased out in favor of electronically read out detectors.

The Gargamelle [187] detector at CERN used Freon and propane gas targets to make the first observation of neutrino-induced NC interactions and more. The BEBC [188] detector at CERN was a bubble chamber that was alternately filled with liquid hydrogen, deuterium, and a neon-hydrogen mixture; BEBC was also outfitted with a track-sensitive detector to improve event tagging, and sometimes used with a small emulsion chamber. The SKAT [192] heavy freon bubble chamber was exposed to wideband neutrino and antineutrino beams at the Serpukhov laboratory in the former Soviet Union. A series of American bubble chambers in the 1970's and 1980's made measurements on free nucleons that are still crucial inputs for neutrino-nucleus scattering predictions. The 12-foot bubble chamber at ANL [189] in the USA used both deuterium and hydrogen targets, as did the 7-foot bubble chamber at BNL [190]. Fermilab's 15 foot bubble chamber [191] used deuterium and heavy neon targets.

34.10.3.3. *Iron Tracking Calorimeters:*

Because of the forward boost of high energy interactions, long detectors made of magnetized iron interspersed with active detector layers have been very successfully employed. The long magnetized detectors allow measurements of the momentum of penetrating muons. The iron planes also act as shower-inducing layers, allowing separation of EM and hadronic showers; the large number of iron planes provide enough mass for high statistics and/or shower containment. Magnetized iron spectrometers have been used for studies of the weak interaction, measurements of structure functions, and searches for neutrino oscillation. Non-magnetized iron detectors have also been successfully employed as neutrino monitors for oscillation experiments and also for neutrino-nucleus interaction studies.

The CDHS [201] detector used layers of magnetized iron modules interspersed with wire drift chambers, with a total (fiducial) mass of 1250 t (750 t), to detector neutrinos in the range 30–300 GeV. Within each iron module, 5 cm (or 15 cm) iron plates were interspersed with scintillation counters. The FNAL Lab-E neutrino detector was used by the CCFR [202] and NuTeV [203] collaborations to

perform a series of experiments in the Fermilab high energy neutrino beam (50 GeV$< E_\nu <$ 300 GeV). The detector was comprised of six iron target calorimeter modules, with 690 t total target mass, followed by three muon spectrometer modules, followed by two drift chambers. Each iron target calorimeter module comprised 5.2 cm thick steel plates interspersed with liquid scintillation counters and drift chambers. The muon spectrometer was comprised of toroidal iron magnets interleaved with drift chambers. The MINOS [204] detectors, a near detector of 980 t at FNAL and a far detector of 5400 t in the Soudan mine, are functionally identical magnetized iron calorimeters, comprised of iron plates interleaved with layers of 4 cm wide plastic scintillator strips in alternating orientations. The T2K [222] on-axis detector, INGRID, consists of 16 non-magnetized iron scintillator sandwich detectors, each with nine 6.5 cm iron plane (7.1 t total) interspersed between layers of 5 cm wide plastic scintillator strips readout out by multi-pixel photon counters (MPPCs) coupled to WLS fibers. Fourteen of the INGRID modules are arranged in a cross-hair configuration centered on the neutrino beam axis.

34.10.3.4. *Cherenkov Detectors:*

Open volume water Cherenkov detectors were originally built to search for proton decay. Large volumes of ultra-pure water were lined with photomultipliers to collect Cherenkov light emitted by the passage of relativistic charged particles. See Sec. 35.3.1 for a detailed discussion of deep liquid detectors for rare processes.

When used to detect $\sim$ GeV neutrinos, the detector medium acts as a natural filter for final state particles below the Cherenkov threshold; this feature has been exploited successfully by the K2K, MiniBooNE (using mineral oil instead of water), and T2K neutrino oscillation experiments. However, at higher energies Cherenkov detectors become less accurate because the overlapping rings from many final state particles become increasingly difficult to resolve.

The second-generation Cherenkov detector in Japan, Super-Kamiokande [193](Super-K), comprises 50 kt (22.5 kt fiducial) of water viewed by 11,146 50 cm photomultiplier tubes, giving 40% photocathode coverage; it is surrounded by an outer detector region viewed by 1,885 20 cm photomultipliers. Super-K is the far detector for K2K and T2K, and is described in greater detail elsewhere in this review. The K2K experiment also employed a 1 kt water Cherenkov detector in the suite of near detectors [194], with 690 photomultipliers (40% photocathode coverage) viewing the detector volume. The MiniBooNE detector at FNAL was a 0.8 kt [195] mineral oil Cherenkov detector, with 1,520 20 cm photomultipliers (10% photocathode coverage) surrounded by a veto detector with 240 20 cm photomultipliers.

34.10.3.5. *Scintillation Detectors:*

Liquid and solid scintillator detectors also employ fully (or nearly fully) active detector media. Typically organic scintillators, which emit into the ultraviolet range, are dissolved in mineral oil or plastic and read out by photomultipliers coupled to wavelength shifters (WLS). Open volume scintillation detectors lined with photomultipliers are conceptually similar to Cherenkov detectors, although energy reconstruction is calorimetric in nature as opposed to kinematic (see also Sec. 35.3.1). For higher energies and higher particle multiplicities, it becomes beneficial to use segmented detectors to help distinguish particle tracks and showers from each other.

The LSND [197] detector at LANL was an open volume liquid scintillator detector (of mass 167 t) employed to detect relatively low energy (<300 MeV) neutrinos. The NOνA [200] detectors use segmented volumes of liquid scintillator in which the scintillation light is collected by WLS fibers in the segments that are coupled to avalanche photodiodes (APDs) at the ends of the volumes. The NOνA far detector, located in Ash River, MN, is comprised of 896 layers of 15.6 m long extruded PVC scintillator cells for a total mass of 14 kt; the NOνA near detector is comprised of 214 layers of 4.1 m scintillator volumes for a total mass of of 300 t. Both are placed in the NuMI beamline at 0.8° off-axis. The SciBar (Scintillation Bar) detector was originally built for K2K at KEK in Japan and then re-used for SciBooNE [198] at FNAL. SciBar used plastic scintillator strips with 1.5 cm×2.5 cm rectangular cross section, read out by multianode photomultipliers (MAPMTs) coupled to WLS fibers, arranged in alternating horizontal and vertical layers, with a total mass of 15 t. Both SciBooNE and K2K employed an EM calorimeter downstream of SciBar and a muon range detector (MRD) downstream of that. The MINERvA [199] detector, in the NuMI beam at FNAL, utilizes a central tracker comprising 8.3 t of plastic scintillator strips with triangular cross section, and is also read out by MAPMTs coupled to WLS fibers. MINERvA employs several more subsystems and is described more fully below.

34.10.3.6. *Liquid Argon Time Projection Chambers:*

Liquid argon time projection chambers (LAr-TPCs) were conceived in the 1970s as a way to achieve a fully active detector with sub-centimeter track reconstruction [205]. A massive volume of purified liquid argon is put under a strong electric field (hundreds of V/cm), so that the liberated electrons from the paths of ionizing particles can be drifted to the edge of the volume and read out, directly by collecting charge from wire planes or non-destructively through charge induction in the wire planes. A dual-phase readout method is also being developed, in which the charge is drifted vertically and then passed through an amplification region inside a gas volume above the liquid volume; the bottom of the liquid volume is equipped with a PMT array for detecting scintillation photons form the liquid argon. The first large scale LAr-TPC was the ICARUS T-600 module [206], comprising 760 t of liquid argon with a charge drift length of 1.5 m read out by wires with 3 mm pitch, which operated in LNGS, both standalone and also exposed to the CNGS high energy neutrino beam. The ArgoNeuT [207] detector at FNAL, with fiducial mass 25 kg of argon read out with 4 mm pitch wires, was exposed to the NuMI neutrino and antineutrino beams. The MicroBooNE [208] detector at FNAL comprises 170 t of liquid Ar, read out with 3 mm wire pitch, which began collecting data in the Booster Neutrino Beam Oct 2015. A LAr-TPC has also been chosen as the detector design for the future DUNE neutrino oscillation experiment, from FNAL to Sanford Underground Research Facility; both single and dual phase modules are planned.

34.10.3.7. *Emulsion Detectors:*

Photographic film emulsions have been employed in particle physics experiments since the 1940s [209]. Thanks to advances in scanning technology and automation [213], they have been successfully employed as neutrino detectors. Emulsions are used for experiments observing CC tau neutrino interactions, where the short lifetime of the tau, $\tau_\tau = 2.90 \times 10^{-13}$s, leading to the short mean path length, $c \times \tau = 87\mu$m, requires extremely precise track resolution. They are employed in hybrid detectors in which the emulsion bricks are embedded inside fine-grained tracker detectors. In the data analysis, the tracker data are used to select events with characteristics typical of a tau decay in the final state, such as missing energy and unbalanced transverse momentum. The reconstructed tracks are projected back into an emulsion brick and used as the search seed for a neutrino interaction vertex.

E531 [210] at Fermilab tested many of the emulsion-tracker hybrid techniques employed by later neutrino experiments, in a detector with approximately 9 kg of emulsion target. The CHORUS [211] experiment at CERN used 1,600 kg of emulsion, in a hybrid detector with a fiber tracker, high resolution calorimeter, and muon spectrometer, to search for $\nu_\mu \to \nu_\tau$ oscillation. The DONuT [212] experiment at FNAL used a hybrid detector, with 260 kg of emulsion bricks interspersed with fiber trackers, followed by a magnetic spectrometer, and calorimeter, to make the first direct observation of tau neutrino CC interactions. More recently, the OPERA [214,215,216] experiment used an automated hybrid emulsion detector, with 1,300 t of emulsion, to make the first direct observation of the appearance of ν_τ in a ν_μ beam.

34.10.3.8. *Hybrid Detectors:*

The CHARM detector [217] at CERN was built to study neutral-current interactions and search for muon neutrino oscillation. It was a fine-grained ionization calorimeter tracker with approximately 150 t of marble as neutrino target, surrounded by a magnetized iron muon system for tagging high angle muons, and followed downstream by a muon spectrometer. The CHARM II detector [218] at CERN comprised a target calorimeter followed by a downstream muon spectrometer. Each target calorimeter module consists of a 4.8 cm thick glass plate followed by a layer of plastic streamer tubes, with spacing 1 cm, instrumented with 2 cm wide pickup strips. Every fifth module is followed by a 3 cm thick scintillator layer. The total mass of the target calorimeter was 692 t.

The Brookhaven E-734 [219] detector was a tracking calorimeter made up of 172 t liquid scintillator modules interspersed with proportional drift tubes, followed by a dense EM calorimeter and a muon spectrometer downstream of that. The detector was exposed to a wideband horn-focused beam with peak neutrino energy near 1 GeV. The Brookhaven E-776 [220] experiment comprised a finely segmented EM calorimeter, with 2.54 cm concrete absorbers interspersed with planes of drift tubes and acrylic scintillation counters, with total mass 240 t, followed by a muon spectrometer.

The NOMAD [221] detector at CERN consisted of central tracker detector inside a 0.4 T dipole magnet (the magnet was originally used by the UA1 experiment at CERN) followed by a hadronic calorimeter and muon detectors downstream of the magnet. The main neutrino target is 3 t of drift chambers followed downstream by transition radiation detectors which are followed by an EM calorimeter. NOMAD was exposed to the same wideband neutrino beam as was CHORUS.

MINERvA, introduced above, is, in its entirety, a hybrid detector, based around a central plastic scintillator tracker. The scintillator tracker is surrounded by electromagnetic and hadronic calorimetry, which is achieved by interleaving thin lead (steel) layers between the scintillator layers for the ECAL (HCAL). MINERvA is situated upstream of the MINOS near detector which acts as a muon spectrometer. Upstream of the scintillator tracker is a nuclear target region containing inactive layers of C (graphite), Pb, Fe (steel), and O (water). MINERvA's physics goals span a wide range of neutrino-nucleus interaction studies, from form factors to nuclear effects.

T2K [222] in Japan employs two near detectors at 280 m from the neutrino beam target, one centered on the axis of the horn-focused J-PARC neutrino beam and one placed 2.5° off-axis. The on-axis detector, INGRID, is described above. The 2.5° off-axis detector, ND280, employs the UA1 magnet (at 0.2 T) previously used by NOMAD. Inside the magnet volume are three separate detector systems: the trackers, the Pi0 Detector (P0D), and several ECal modules. The tracker detectors comprise two fine-grained scintillator detectors (FGDs), read out by MPPCs coupled to WLS fibers, interleaved between three gas TPCs read out by micromegas planes. The downstream FGD contains inactive water layers in addition to the scintillators. Upstream of the tracker is the P0D, a sampling tracker calorimeter with active detector materials comprising plastic scintillator read out by MPPCs and WLS fibers, and inactive sheets of brass radiators and refillable water modules. Surrounding the tracker and P0D, but still inside the magnet, are lead-scintillator EM sampling calorimeters.

34.11. Superconducting magnets for collider detectors

Revised September 2015 by Y. Makida (KEK)

34.11.1. ***Solenoid Magnets*** : In all cases SI unit are assumed, so that the magnetic field, B, is in Tesla, the stored energy, E, is in joules, the dimensions are in meters, and $\mu_0 = 4\pi \times 10^{-7}$.

The magnetic field (B) in an ideal solenoid with a flux return iron yoke, in which the magnetic field is < 2 T, is given by

$$B = \frac{\mu_0 \, n \, I}{L} \tag{34.39}$$

where n is the number of turns, I is the current and L is the coil length. In an air-core solenoid, the central field is given by

$$B(0,0) = \mu_0 \, n \, I \frac{L}{\sqrt{L^2 + 4R^2}} \ , \tag{34.40}$$

where R is the coil radius.

In most cases, momentum analysis is made by measuring the circular trajectory of the passing particles according to $p = mv = qrB$, where p is the momentum, m the mass, q the charge, r the bending radius. The sagitta, s, of the trajectory is given by

$$s = q \, B \, \ell^2 / 8p \ , \tag{34.41}$$

where ℓ is the path length in the magnetic field. In a practical momentum measurement in colliding beam detectors, it is more effective to increase the magnetic volume than the field strength, since

$$dp/p \propto p / B \, \ell^2 \ , \tag{34.42}$$

where ℓ corresponds to the solenoid coil radius R. The energy stored in the magnetic field of any magnet is calculated by integrating B^2 over all space:

$$E = \frac{1}{2\mu_0} \int B^2 dV \tag{34.43}$$

If the coil thin and inside an iron return yoke , (which is the case if it is to superconducting coil), then

$$E \approx (B^2/2\mu_0)\pi R^2 L \ . \tag{34.44}$$

For a detector in which the calorimetry is outside the aperture of the solenoid, the coil must be thin in terms of radiation and absorption lengths. This usually means that the coil is superconducting and that the vacuum vessel encasing it is of minimum real thickness and fabricated of a material with long radiation length. There are two major contributors to the thickness of a thin solenoid:

1) The conductor consisting of the current-carrying superconducting material (usually Nb-Ti/Cu) and the quench protecting stabilizer (usually aluminum) are wound on the inside of a structural support cylinder (usually aluminum also). The coil thickness scales as B^2R, so the thickness in radiation lengths (X_0) is

$$t_{\rm coil}/X_0 = (R/\sigma_h X_0)(B^2/2\mu_0) \ , \tag{34.45}$$

where $t_{\rm coil}$ is the physical thickness of the coil, X_0 the average radiation length of the coil/stabilizer material, and σ_h is the hoop stress in the coil [225]. $B^2/2\mu_0$ is the magnetic pressure. In large detector solenoids, the aluminum stabilizer and support cylinders dominate the thickness; the superconductor (Nb-TI/Cu) contributes a smaller fraction. The main coil and support cylinder components typically contribute about 2/3 of the total thickness in radiation lengths.

2) Another contribution to the material comes from the outer cylindrical shell of the vacuum vessel. Since this shell is susceptible to buckling collapse, its thickness is determined by the diameter, length and the modulus of the material of which it is fabricated. The outer vacuum shell represents about 1/3 of the total thickness in radiation length.

(2007);
T.Kim *et al.*, Nucl. Instrum. Methods **A599**, 173 (2008).
103. M. Chefdeville *et al.*, Nucl. Instrum. Methods **A556**, 490 (2006).
104. M. Titov, arXiv:physics/0403055 (2004).
105. http://rd51-public.web.cern.ch/RD51-Public.
106. J. Alme *et al.*, Nucl. Instrum. Methods **A622**, 316 (2010).
107. N. Abgrall *et al.*, Nucl. Instrum. Methods **A637**, 25 (2011).
108. ALICE Collab., ALICE-PUBLIC-2015-004 (2015).
109. A.H. Walenta *et al.*, Nucl. Instrum. Methods **161**, 45 (1979).
110. H. Aihara *et al.*, IEEE Trans. **NS30**, 63 (1983).
111. X. Artru *et al.*, Phys. Rev. **D12**, 1289 (1975);
G.M. Garibian *et al.*, Nucl. Instrum. Methods **125**, 133 (1975).
112. B. Dolgoshein, Nucl. Instrum. Methods **A326**, 434 (1993).
113. *TRDs for the Third Millenium: Proc. 2nd Workshop on Advanced Transition Radiation Detectors for Accelerator and Space Applications*, Nucl. Instrum. Methods **A522**, 1 (2004).
114. *TRDs for the Third Millenium: Proc. 4th Workshop on Advanced Transition Radiation Detectors for Accelerator and Space Applications*, Nucl. Instrum. Methods **A706**, 1 (2013).
115. B. Beischer *et al.*, Nucl. Instrum. Methods **A583**, 485 (2007).
116. A. Adronic and J.P Wessels, Nucl. Instrum. Methods **A666**, 130 (2012).
117. M. Petris *et al.*, Nucl. Instrum. Methods **A714**, 17 (2007).
118. J. Apostolakis *et al.*, Rad. Phys. and Chem. **78**, 859 (2009).
119. R. Santonico and R. Cardarelli, Nucl. Instrum. Methods **A187**, 377 (1981).
120. V.V. Parkhomchuck, Yu.N. Pestov, and N.V. Petrovykh, Nucl. Instrum. Methods **93**, 269 (1971).
121. E. Cerron Zeballos *et al.*, Nucl. Instrum. Methods **A374**, 132 (1996).
122. R. Cardarelli *et al.*, Nucl. Instrum. Methods **A333**, 399 (1993).
123. P. Camarri *et al.*, Nucl. Instrum. Methods **A414**, 317 (1998).
124. G. Aielli *et al.*, Nucl. Instrum. Methods **A508**, 6 (2003).
125. R. Cardarelli *et al.*, Nucl. Instrum. Methods **A382**, 470 (1996).
126. R. Cardarelli *et al.*, JINST **8**, P01003 (2013).
127. G. Aielli *et al.*, JINST **9**, C09030 (2014).
128. R. Santonico, JINST **9**, C11007 (2014).
129. R. Santonico *et al.*, Nucl. Instrum. Methods **A661**, S2 (2012).
130. M. Bedjidian *et al.*, JINST **6** P02001 (2011).
131. P. Fonte *et al.*, Nucl. Instrum. Methods **A443**, 201 (2000).
132. L. Paolozzi *et al.*, PoS(RPC2012)065 (2012).
133. S. An *et al.*, Nucl. Instrum. Methods **A594**, 39 (2008).
134. C. Iacobaeus *et al.*, Nucl. Instrum. Methods **A513**, 244 (2003).
135. G. Aielli *et al.*, Nucl. Instrum. Methods **A456**, 82 (2000).
136. G. Aielli *et al.*, IEEE Trans. **NS53**, 567 (2006).
137. H. Sakai *et al.*, Nucl. Instrum. Methods **A484**, 153 (2002).
138. R. Santonico, JINST **8**, P04023 (2013).
139. L. Lopes *et al.*, Nucl. Instrum. Methods **A533**, 69 (2003).
140. H. Spieler, *Semiconductor Detector Systems*, Oxford Univ. Press, Oxford (2005).
141. F. Scholze *et al.*, Nucl. Instrum. Methods **A439**, 208 (2000).
142. G. Lindström *et al.*, Nucl. Instrum. Methods **A465**, 60 (2001).
143. C. Da Via *et al.*, Nucl. Instrum. Methods **A509**, 86 (2003).
144. G. Kramberger *et al.*, Nucl. Instrum. Methods **A481**, 297 (2002).
145. O. Krasel *et al.*, IEEE Trans. **NS51**, 3055 (2004).
146. G. Lindström *et al.*, Nucl. Instrum. Methods **A426**, 1 (1999).
147. A. Holmes-Siedle and L. Adams, *Handbook of Radiation Effects*, 2nd edition, Oxford Univ. Press, Oxford (2002).
148. V. Radeka, IEEE Trans. **NS15**, 455 (1968);
V. Radeka, IEEE Trans. **NS21**, 51 (1974).
149. F.S. Goulding, Nucl. Instrum. Methods **100**, 493 (1972);
F.S. Goulding and D.A. Landis, IEEE Trans. **NS29**, 1125 (1982).
150. W.R. Nelson, H. Hirayama, and D.W.O. Rogers, SLAC-265 (1985).
151. R. Brun *et al.*, CERN DD/EE/84-1 (1987).
152. D. Hitlin *et al.*, Nucl. Instrum. Methods **137**, 225 (1976);
See also W. J. Willis and V. Radeka, Nucl. Instrum. Methods **120**, 221 (1974), for a more detailed discussion.
153. R. Wigmans, *Calorimetry: Energy Measurement in Particle Physics*, Inter. Series of Monographs on Phys. **107**, Clarendon Press, Oxford (2000).
154. ATLAS Collab., CERN/LHCC 96-41 (1996).
155. CMS Collab., CERN/LHCC 97-33 (1997).
156. N. Akchurin *et al.*, Nucl. Instrum. Methods **A399**, 202 (1997).
157. B. Aubert *et al.*, Nucl. Instrum. Methods **A321**, 467 (1992).
158. A. Artamonov *et al.*, JINST **3**, P02010 (2008).
159. F. Ariztizabal *et al.*, Nucl. Instrum. Methods **A349**, 384 (1994).
160. S. Abdullin *et al.*, Eur. Phys. J. **C53**, 139 (2008).
161. M. Romalli, J. Phys. Conf. Series **404** 012050 (2012);
C. Adloff *et al.*, arXiv:1306.3037 (2013).
162. T.A. Gabriel *et al.*, Nucl. Instrum. Methods **A338**, 336 (1994).
163. D.E. Groom, Nucl. Instrum. Methods **A572**, 633 (2007);
Erratum: D.E. Groom, Nucl. Instrum. Methods **A593**, 638 (2008).
164. N. Akchurin *et al.*, Nucl. Instrum. Methods **A408**, 380 (1998);
An energy-independent analysis of these data is given in Ref. 163.
165. P. Adragna *et al.*, Nucl. Instrum. Methods **A615**, 158 (2010).
166. C.W. Fabjan *et al.*, Phys. Lett. **B60**, 105 (1975).
167. C. Leroy, J. Sirois, and R. Wigmans, Nucl. Instrum. Methods **A252**, 4 (1986).
168. J.E. Brau and T.A. Gabriel, Nucl. Instrum. Methods **A238**, 489 (1985);
H. Brückmann and H. Kowalski, ZEUS Int. Note 86/026 DESY, Hamburg (1986);
R. Wigmans, Nucl. Instrum. Methods **A259**, 389 (1987);
R. Wigmans, Nucl. Instrum. Methods **A265**, 273 (1988).
169. P. Mockett, SLAC-267, 335 (1987).
170. R. Wigmans, *Proc. 7th Inter. Conf. on Calorimetry in High Energy Physics*, 182 World Scientific, River Edge, NJ, (1998);
N. Akchurin *et al.*, Nucl. Instrum. Methods **A537**, 537 (2005).
171. G. Drews *et al.*, Nucl. Instrum. Methods **A335**, 335 (1990).
172. M. Holder *et al.*, Nucl. Instrum. Methods **151**, 69 (1978).
173. R.K. Bock, T. Hansl-Kozanecka, and T.P. Shah, Nucl. Instrum. Methods **186**, 533 (1981);
Y.A. Kulchitsky and V.B. Vinogradov, Nucl. Instrum. Methods **A455**, 499 (2000).
174. D. Acosta *et al.*, Nucl. Instrum. Methods **A316**, 184 (1997).
175. N. Akchurin, *et al.*, Nucl. Instrum. Methods **A735**, 120 (2013).
176. W. Walkowiak, Nucl. Instrum. Methods **A449**, 288 (2000).
177. L.S. Miller *et al.*, Phys. Rev. **166**, 871 (1968).
178. E. Shibamura *et al.*, Nucl. Instrum. Methods **A316**, 184 (1975).
179. K. Yoshino *et al.*, Phys. Rev. **A14**, 438 (1976).
180. A.O. Allen *et al.*, NSRDS-NBS-58 (1976).
181. P. Benetti *et al.*, Nucl. Instrum. Methods **A32**, 361 (1993).
182. A.M. Kalinin *et al.*, ATLAS-LARG-NO-058 (1996).
183. G. Danby *et al.*, Phys. Rev. Lett. **9**, 36 (1962).
184. S. van der Meer, CERN 61-07 (1961).
185. J.A. Formaggio and G.P. Zeller, Rev. Mod. Phys. **84**, 1307 (2013).
186. H. Faissner *et al.*, Phys. Lett. **B68**, 377 (1977).
187. F.J. Hasert *et al.*, Nucl. Phys. **B73**, 1 (1974).
188. N. Armenise *et al.*, Phys. Lett. **B81**, 385 (1979).
189. S.J. Barish *et al.*, Phys. Rev. **D16**, 3103 (1977).
190. N.J. Baker *et al.*, Phys. Rev. **D23**, 2499 (1981).
191. J.W. Chapman *et al.*, Phys. Rev. **D14**, 5 (1976).
192. A.E. Asratien *et al.*, Phys. Lett. **79**, 497 (1978).
193. Y. Fukuda *et al.*, Nucl. Instrum. Methods **A501**, 418 (2003).
194. Y. Fukuda *et al.*, Phys. Rev. **D74**, 072003 (2006).
195. A.A. Aguilar-Arevalo *et al.*, Nucl. Instrum. Methods **A599**, 28 (2009).
196. A.A. Aguilar-Arevalo *et al.*, Phys. Rev. **D79**, 072002 (2009).
197. C. Athanassopoulos *et al.*, Nucl. Instrum. Methods **A388**, 149 (1997).
198. K. Hiraide *et al.*, Phys. Rev. **D78**, 112004 (2008).
199. L. Aliaga *et al.*, Nucl. Instrum. Methods **A743**, 130 (2014).
200. D.S. Ayres *et al.*, FERMILAB-DESIGN-2007-01 (2007).
201. M. Holder *et al.*, Nucl. Instrum. Methods **148**, 203 (1978).

202. W.K. Sakumoto *et al.*, Nucl. Instrum. Methods **A294**, 179 (1990).
203. D.A. Harris *et al.*, Nucl. Instrum. Methods **A447**, 377 (2000).
204. I. Ambats *et al.*, FERMILAB-DESIGN-1998-02 (1998).
205. C. Rubbia, CERN-EP-INT-77-08 (1977).
206. S. Amerio *et al.*, Nucl. Instrum. Methods **A527**, 329 (2004).
207. C. Anderson *et al.*, JINST **7**, 10020 (2012).
208. H. Chen *et al.*, FERMILAB-PROPOSAL-0974 (2007).
209. D.H. Perkins, Nature **159**, 126 (1947).
210. N. Uhida *et al.*, Nucl. Instrum. Methods **224**, 50 (1984).
211. S. Aoki *et al.*, Nucl. Instrum. Methods **A447**, 361 (2000).
212. K. Kodama *et al.*, Nucl. Instrum. Methods **B93**, 340 (1994).
213. S. Aoki, Nucl. Instrum. Methods **A473**, 192 (2001).
214. T. Adam *et al.*, Nucl. Instrum. Methods **A577**, 523 (2007).
215. D. Di Ferdinando *et al.*, Radiat. Meas. **44**, 840 (2009).
216. R. Acquafredda *et al.*, New J. Phys. **8**, 303 (2006).
217. A.N. Diddens *et al.*, Nucl. Instrum. Methods **178**, 27 (1980).
218. D. Geiregat *et al.*, Nucl. Instrum. Methods **A325**, 92 (1993).
219. L.A. Ahrens *et al.*, Nucl. Instrum. Methods **A254**, 515 (1987).
220. G. Gidal, LBL-91 Suppl., Rev. (1985).
221. J. Altegoer *et al.*, Nucl. Instrum. Methods **A404**, 96 (1998).
222. K. Abe *et al.*, Nucl. Instrum. Methods **A659**, 106 (2011).
223. T. Taylor, Phys. Scripta **23**, 459 (1980).
224. A. Yamamoto, Nucl. Instrum. Methods **A494**, 255 (2003).
225. A. Yamamoto, Nucl. Instrum. Methods **A453**, 445 (2000).
226. R.L. Gluckstern, Nucl. Instrum. Methods **24**, 381 (1963).
227. V. Karimäki, Nucl. Instrum. Methods **A410**, 284 (1998).